The Role of Serine 167 in Human Indoleamine 2,3-Dioxygenase: A Comparison with Tryptophan 2,3-Dioxygenase[†]

Nishma Chauhan,[‡] Jaswir Basran,[§] Igor Efimov,[‡] Dimitri A. Svistunenko,[||] Harriet E. Seward,[§] Peter C. E. Moody,[§] and Emma Lloyd Raven*[,‡]

Department of Chemistry, University of Leicester, University Road, Leicester LE1 7RH, England, Department of Biochemistry, University of Leicester, Lancaster Road, Leicester LE1 9HN, England, and Department of Biological Sciences, University of Essex, Wivenhoe Park, Colchester CO4 3SQ, England

Received December 8, 2007; Revised Manuscript Received February 7, 2008

ABSTRACT: The initial step in the L-kynurenine pathway is oxidation of L-tryptophan to *N*-formylkynurenine and is catalyzed by one of two heme enzymes, tryptophan 2,3-dioxygenase (TDO) or indoleamine 2,3-dioxygenase (IDO). Here, we address the role of the conserved active site Ser167 residue in human IDO (S167A and S167H variants), which is replaced with a histidine in other mammalian and bacterial TDO enzymes. Our kinetic and spectroscopic data for S167A indicate that this residue is not essential for O_2 or substrate binding, and we propose that hydrogen bond stabilization of the catalytic ferrous−oxy complex involves active site water molecules in IDO. The data for S167H show that the ferrous−oxy complex is dramatically destabilized in this variant, which is similar to the behavior observed in human TDO [Basran et al. (2008) *Biochemistry 47*, 4752−4760], and that this destabilization essentially destroys catalytic activity. New kinetic data for the wild-type enzyme also identify the ternary [enzyme−O_2−substrate] complex. The data reveal significant differences between the IDO and TDO enzymes, and the implications of these results are discussed in terms of our current understanding of IDO and TDO catalysis.

The initial, rate-limiting step in the L-kynurenine pathway is the oxidative cleavage of L-tryptophan to *N*-formylkynurenine (Scheme 1) and is catalyzed by one of two heme dioxygenase enzymes, indoleamine 2,3-dioxygenase (IDO)[1] or tryptophan 2,3-dioxygenase (TDO). Although they catalyze the same reaction, TDO and IDO are otherwise distinct, and we know little about their structure and mechanism.

The first detailed structural and functional information that appeared was for human indoleamine 2,3-dioxygenase. A recent crystal structure for ferric human IDO (*1*) reveals an active site that is much more hydrophobic than for other, well-characterized O_2-dependent heme enzymes (Figure 1A) and which is presumably configured to encourage binding of the hydrophobic substrate. Subsequently, a structure for the bacterial *Xanthomonas campestris* TDO (xTDO) in complex with L-Trp (*2*) was published (Figure 1B,C) and indicated that an active site histidine, His55, hydrogen bonds to the indole nitrogen of the substrate in the substrate-bound complex (Figure 1C).

Scheme 1: Reaction Catalyzed by IDO, with IUPAC Numbering Indicated

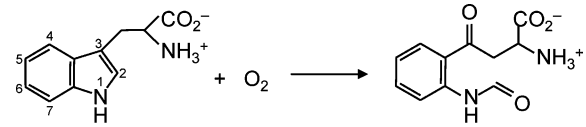

Although these structures have provided critical insight into the molecular details of the active site architecture and the substrate binding interactions, they also raise a number of important questions for which there are currently no satisfactory answers. To begin with, the most striking feature of the IDO active site is that, with the notable exception of Ser167, it is almost devoid of polar residues (Figure 1A). This marks IDO as distinct from some other heme proteins (e.g., the globins and peroxidases), which often have an active site histidine residue in the distal pocket that provides hydrogen-bonding stabilization to ligands bound at the heme iron. The first questions that arise, therefore, are whether similar hydrogen-bonding stabilization of the ferrous−oxy species is required during IDO catalysis, how is this provided, and whether this applies universally across the heme dioxygenase family. A second notable difference between xTDO and IDO is that the critical His55 residue is missing in IDO, replaced by a serine residue at position 167 that is conserved across all IDOs (Figure 1). Sequence alignments indicate that this active site histidine is similarly conserved among all

[†] This work was supported by grants from The Leverhulme Trust (fellowship to E.L.R.), BBSRC (grants BB/C00602X/1 and IIP0206/009), and EPSRC (studentship to N.C.).

* To whom correspondence should be addressed. Telephone: +44 (0)116 229 7047. Fax: +44 (0)116 252 3789. E-mail: emma.raven@le.ac.uk.

[‡] Department of Chemistry, University of Leicester.

[§] Department of Biochemistry, University of Leicester.

[||] Department of Biological Sciences, University of Essex.

[1] Abbreviations: IDO, indoleamine 2,3-dioxygenase; rhIDO, recombinant human indoleamine 2,3-dioxygenase; L-Trp, L-tryptophan; TDO, tryptophan 2,3-dioxygenase; rhTDO, recombinant human tryptophan 2,3-dioxygenase; xTDO, *Xanthomonas campestris* tryptophan 2,3-dioxygenase.

10.1021/bi702405a CCC: $40.75
Published on Web 03/28/2008

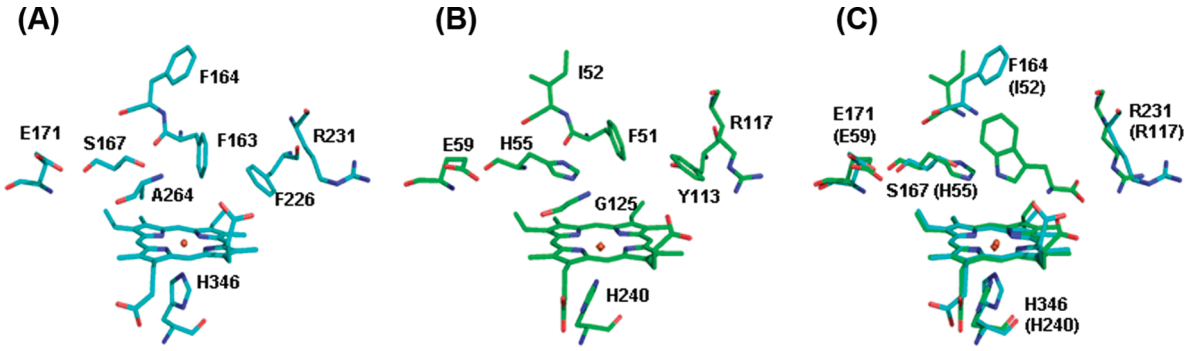

FIGURE 1: Comparison of the active sites of IDO and TDO. (A) The active site of rhIDO [in cyan (*1*)]. (B) The active site of xTDO [in green (*2*)] in the same orientation as that shown for rhIDO. Active site residues for rhIDO are H346, R231, F226, F163, S167, A264, F164, and E171 which correspond to H240, R117, Y113, F51, H55, G125, I52, and E59 in xTDO. (C) An overlay of rhIDO (cyan) and the xTDO−Trp (green) complex with the residues for rhIDO indicated and those for xTDO in parentheses.

TDOs isolated to date (*3*) (including human TDO), raising the question as to its specific role in the reaction mechanism.

In this paper, we sought answers to these questions in recombinant human IDO (rhIDO) by means of a direct comparison with the TDO enzymes (S167A and S167H variants in rhIDO). Together with the data presented for human tryptophan 2,3-dioxygenase in the preceding paper (*4*), the results reveal important differences in reactivity between different dioxygenases, and the data are discussed in terms of our wider understanding of the reaction mechanism in this family of enzymes.

EXPERIMENTAL PROCEDURES

Materials. L-Tryptophan and all of the chemicals used for buffers (Sigma-Aldrich) were of the highest analytical grade (more than 99% purity) and were used without further purification. Aqueous solutions were prepared using water purified through an Elgastat option 2 water purifier, which itself was fed with deionized water. All pH measurements were made using a Russell pH electrode attached to a digital pH meter (Radiometer Copenhagen, model PHM 93).

Mutagenesis and Protein Purification. Site-directed mutagenesis on rhIDO was performed according to the QuikChange protocol (Stratagene Ltd., Cambridge, U.K.). Bacterial fermentation of cells and purification of rhIDO, S167A, and S167H mutants were carried out according to published procedures (*5*) with the exception that, after sonication, 5 mg of DNase I and 20 mM $MgCl_2$ were added and the suspension was stirred for a further 30 min at 4 °C. Absorption coefficients for S167A ($\epsilon_{404} = 144$ mM^{-1} cm^{-1}) and S167H ($\epsilon_{408} = 166$ mM^{-1} cm^{-1}) were determined using the pyridine hemochromagen method (*6*); for rhIDO, $\epsilon_{404} = 172$ mM^{-1} cm^{-1} (*5*). Ligand-bound derivatives (azide, cyanide, and fluoride) were obtained by the addition (typically 2–10 μL) of a concentrated (1 M) solution of ligand to the ferric enzyme. The ferrous−oxy derivative was generated by direct bubbling of O_2 gas through a dithionite-reduced sample of enzyme.

Equilibrium Binding Constants. Equilibrium dissociation constants (50 mM Tris-HCl, pH 8.0, 25.0 ± 0.1 °C), K_D, for binding of both L-Trp and cyanide were determined according to published procedures (*7*). Binding of L-Trp to ferric rhIDO and S167A in the presence of cyanide was carried out on samples of ferric rhIDO and S167A saturated with 80 and 20 μM cyanide, respectively, and absorbance changes were monitored at 416 nm.

EPR Spectroscopy. EPR spectra were recorded using a Bruker EMX EPR spectrometer (X-band) equipped with a spherical high-quality Bruker resonator SP9703 and an Oxford Instruments liquid helium system. The *g*-values were obtained by using the built-in microwave frequency counter and a 2,2-diphenyl-1-picrylhydrazyl standard, the *g*-value for which is 2.0037 ± 0.0002.

Steady-State Measurements. Steady-state oxidation of L-Trp (50 mM Tris-HCl, pH 8.0, 25.0 °C) was carried out using a Perkin-Elmer Lamba 35 UV–visible spectrophotometer according to published protocols (*5*). Initial reaction rates were monitored by following formation of *N*-formylkynurenine as an increase in absorbance at 321 nm ($\epsilon_{321} = 3.75$ mM^{-1} cm^{-1}). The K_M value for O_2 was determined by varying the O_2 concentration (0–300 μM) while keeping the concentration of L-Trp constant and saturating at 200 μM.

Kinetic Measurements. The kinetics of binding of L-Trp, cyanide, and O_2 to rhIDO were determined using an SX.18MV stopped-flow spectrometer housed in an anaerobic glovebox (Belle Technology, $[O_2] < 5$ ppm) and fitted with a Neslab RTE-200 circulating water bath (±0.1 °C). Reported values of k_{obs} are an average of at least four measurements (50 mM Tris-HCl, pH 8.0, 25.0 °C). All reactions were carried out under pseudo-first-order conditions; final (reaction cell) protein concentrations used were 0.5 μM. Absorbance changes accompanying L-Trp and cyanide binding were monitored at 404 nm for rhIDO and S167A and at 408 nm for S167H. For each enzyme−ligand complex the apparent association rate constant (k_{on}) was obtained from the slope of the linear dependence of the observed rate constant, k_{obs}, against ligand concentration; the dissociation rate constant (k_{off}) was obtained from the ordinate intercept of this plot. For O_2 binding experiments, anaerobic conditions were obtained by extensive N_2 equilibration of the buffer and reactions initiated by mixing anaerobic solutions of enzyme (typically 2 μM, prereduced with dithionite) with an equal volume of buffer containing O_2 at different concentrations (0.12−1.2 mM). Formation of the ferrous−oxy complex was monitored at 416 nm. Formation of the ferrous−oxy rhIDO complex was also monitored in the presence of 1-methyl-Trp (300 μM) at the same wavelength.

Detection of Intermediate Species during Reaction of Fe^{2+} with L-Trp and O_2. Time-dependent spectral changes observed during steady-state turnover by IDO were examined by stopped-flow spectroscopy using a photodiode array detector and X-SCAN software (Applied Photophysics). The

sequential mixing mode of the stopped-flow apparatus was used for these experiments. This involved first mixing a solution of ferrous enzyme (1.5 μM) with O_2 (250 μM) with a 1 s (500 ms for S167H) aging time to allow for formation of the ferrous−oxy complex, followed by mixing of the second substrate, L-Trp (50 and 100 μM, respectively, for rhIDO and S167H). The reaction was then monitored for 50 s, and the spectral changes were recorded. The sequential mixing experiment was also carried out where ferrous enzyme was incubated with L-Trp first and then mixed with O_2, and the spectral changes accompanying the reaction were monitored again.

Determination of Fe^{3+}/Fe^{2+} Reduction Potentials. Fe^{3+}/Fe^{2+} reduction potentials for rhIDO, S167A, and S167H were determined by simultaneous reduction with a dye of known potential (*8*) according to previous methodology (*9*). Various dyes were used: nile blue chloride ($E_{m,7} = -116$ mV), phenosafranin ($E_{m,7} = -252$ mV), methylene blue ($E_{m,7} = 11$ mV), and toluidene blue O ($E_{m,7} = 34$ mV). Absorbance changes corresponding to reduction of heme were measured at the isosbestic points for the dyes; nile blue chloride (406 nm), phenosafranin (407 nm), methylene blue (404 nm), and toluidene blue O (400 nm). Reduction of the dye (at the wavelength at which the absorption change due to heme reduction was negligible) was measured at 635 nm for nile blue chloride, 520 nm for phenosafranin, 664 nm for methylene blue, and 637 nm for toluidene blue O. In all cases, linear Nernst plots for one-electron reduction of heme produced the expected slope of 1 across a wide range of potentials, and the intercept gives a reliable value for $\Delta E_{m,7}$ with an error of ±2 mV (*9*). UV–visible spectra obtained in all experiments were analyzed using Specfit (*10*) for singular value decomposition based on factor analysis. All potentials are given versus the normal hydrogen electrode (NHE).

RESULTS

Characterization of S167A and S167H Variants. Analysis of the electronic spectrum of ferric S167A reveals that the wavelength maxima ($\lambda_{max} = 404$, 500, 537, 575, and 628 nm, Figure 2B) are very similar to those for rhIDO ($\lambda_{max} = 404$, 500, 533, and 635 nm, Figure 2A); rhIDO is known to exist as a mixed population of high- and low-spin heme (*5*). For S167H (Figure 2C), the Soret band is red shifted to 408 nm ($\lambda_{max} = 408$, 499, 536, 570, and 628 nm), which is indicative of an increased proportion of low-spin heme, possibly as a result of coordination of His167 to the heme iron.

The spectra of the ferric derivatives of both S167A and S167H did not show any significant dependence on pH over the range examined (pH 6–8); no substantial changes in peak positions or intensities were observed (data not shown). Similar observations have been reported for rhIDO (*5*) and have been attributed to the lack of a proton acceptor in the distal cavity capable of hydrogen bonding to a bound hydroxide in the ferric derivative. A similar arrangement presumably applies for both S167A and S167H.

The electronic spectra of the ferrous derivatives of S167A and S167H are similar to those of rhIDO. This is consistent with the presence of a 5-coordinate heme species in all cases and indicates that the low-spin component in ferric S167H is converted to a high-spin, 5-coordinate heme on reduction.

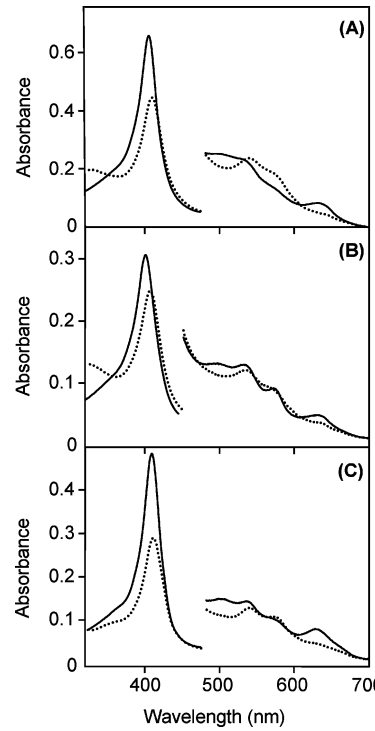

FIGURE 2: UV–visible spectra of (A) rhIDO, (B) S167A, and (C) S167H in the absence (solid line) and presence (dotted line) of L-Trp (20 mM for rhIDO and 40 mM for S167H and S167A). Absorbance values in the visible region have been multiplied by a factor of 5. Reaction conditions: 50 mM Tris-HCl, pH 8.0, 25.0 °C.

Wavelength maxima for other ferric and ferrous derivatives of S167A and S167H in the presence of various exogenous ligands are given in Table 1.

EPR Spectroscopy. EPR spectroscopy was used as a means of providing further information on the heme coordination geometry in S167A and S167H. The EPR spectrum of ferric rhIDO is shown for reference in Figure 3A; axial and rhombic high-spin ($g = 5.82$, 1.99 and 6.17, 5.52, 1.99, respectively) and low-spin ($g = 2.85$, 2.27, 1.62) species have been previously assigned (*5*). The EPR spectrum of S167A (Figure 3B) has an increased proportion of high-spin heme compared to rhIDO, which consists mainly of an axial ($g = 5.85$, 1.99) form.

In contrast, the spectrum of S167H (Figure 3C) contains a major low-spin species ($g = 2.88$, 2.28, and 1.63) which is likely to arise from bishistidine axial ligation in which the imidazole planes are aligned approximately parallel to each other (*11, 12*).

Cyanide Binding. The binding of various noncatalytic ligands to the ferric enzymes is informative because it provides further information on the different coordination environments of the heme. Addition of cyanide gives changes in the visible region that are indicative of the formation of a 6-coordinate low-spin species for both S167A [$\lambda_{max} = 419$, 540, 570 (sh) nm] and S167H [$\lambda_{max} = 418$, 540, 568 (sh) nm] (Table 1). The corresponding binding constants, K_D, are given in Table 2, with spectra shown in Figure 4A. Values of K_D for rhIDO and S167A are broadly similar, but that for S167H is increased by a factor of ≈170, which is in agreement with the spectroscopic data above and consistent with binding of His167 to the iron. Binding of cyanide was also determined kinetically. Second-order rate constants, k_{on}, were derived from a plot of k_{obs} against [cyanide] (Figure

Table 1: Absorption Maxima for rhIDO, S167A, and S167H (50 mM Tris-HCl, pH 8.0, 25.0 °C)

derivative	rhIDO	S167A	S167H
ferric	404, 500, 533, 635	404, 500, 537, 575, 628	408, 500, 536, 570, 628
ferrous	425, 527 sh,[a] 558	426, 529 sh, 557	426, 535 sh, 558
ferrous−oxy	416, 539, 576	416, 539, 576	416, 538, 575
ferric + L-Trp	410, 540, 576	409, 539, 572	409, 539, 573
ferric−azide	413, 535, 572, 643	410, 540, 576, 627	nd[b]
ferric−fluoride	404, 502, 532, 635	405, 500, 537, 575, 628	nd[b]
ferric−cyanide	419, 538, 569 sh	419, 540, 570 sh	418, 540, 568 sh

[a] sh = shoulder. [b] No spectroscopic changes were observed on binding of either azide or fluoride to S167H.

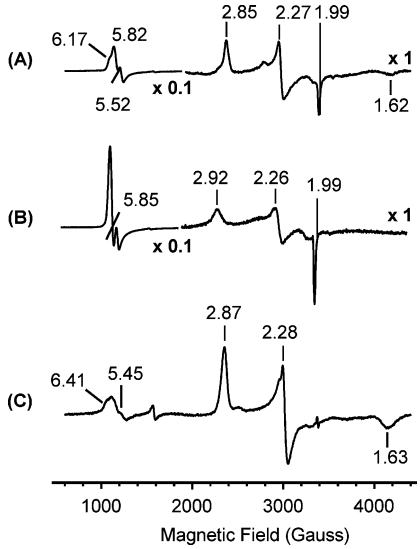

FIGURE 3: EPR spectra of (A) ferric rhIDO, (B) ferric S167A, and (C) ferric S167H. Spectra were measured at 10 K. Experimental conditions: modulation frequency, 100 kHz; microwave frequency, 9.67 GHz; microwave power, 2 mW; modulation amplitude, 10 G. Reaction conditions: 50 mM Tris-HCl, pH 8.0.

4B), and values are given in Table 2. As for the binding data above, the k_{on} value for S167H was ~50 times smaller than for rhIDO. This is informative because it tells us that the weaker K_D for S167H is due to a decreased k_{on}, which is consistent with the bishistidine ligated heme detected by EPR. The k_{on} value obtained for S167A is ≈8-fold faster than for rhIDO.

Substrate Binding. Both S167A and S167H exhibited characteristic spectroscopic changes upon binding of L-Trp at pH 8.0 (Figure 2B,C): the Soret band shifts to 409 nm in both cases. Similar changes in absorbance are observed for rhIDO (Figure 2A) and are consistent with the loss of high-spin heme and the formation of a low-spin, hydroxide-bound species on binding of L-Trp, most likely as a consequence of deprotonation of a water molecule in the active site (*5*). The similarity of the spectroscopic changes for S167A and S167H indicates that binding of substrate occurs in a similar manner and that the corresponding deprotonation of the distal water molecule to form a hydroxide-bound species occurs by a similar mechanism.

Bindings constants, K_D, for binding of L-Trp to S167A and S167H were determined from the above data as 8000 ± 1000 and 6900 ± 1100 μM (pH 8.0), respectively (Table 2). Both of these values are significantly larger than the corresponding value for rhIDO (285 ± 6 μM), although we note that binding of substrate to the ferrous form of both variants (as evidenced by the K_M values, *vide infra*) is similar in all three cases. Pseudo-first-order rate constants, k_{obs}, for binding of L-Trp were fitted to eq 1:

$$k_{obs} = k_{on}[L] + k_{off} \quad (1)$$

Derived rate constants are given in Table 2 and show a marked increase in k_{off} for S167H. Values for K_D (=k_{off}/k_{on}) derived from these data were within error of those determined under equilibrium conditions (data not shown).

Binding constants for binding of L-Trp to the ferric−cyanide complexes were also determined under equilibrium conditions, and derived values of 16.4 ± 1.5 μM for rhIDO and 992 ± 200 μM for S167A were obtained (Table 2). These values are significantly lower than those for the ferric enzyme alone (Table 2) and are indicative of enhanced affinity for L-Trp in the presence of cyanide. The same experiment on the ferric−cyanide complex of S167H gave spectral changes that were much smaller than those for either rhIDO or S167A (both in terms of shift of the Soret band and total change in absorbance). We have interpreted this to mean that binding of L-Trp probably occurs, but the spectroscopic changes were too small to extract a meaningful K_D.

Redox Measurements. The $Fe^{3+/2+}$ reduction potential for S167A was found to be −12 mV (Figure 5A); this compares to a value of −63 mV for rhIDO which was determined using the same method.[2] The $Fe^{3+/2+}$ reduction potential for S167H (−203 mV, Figure 5B) was significantly lower than that for both rhIDO and S167A.

Steady-State Kinetics. Steady-state oxidation of L-Trp at pH 8.0 gave values for k_{cat} = 1.56 ± 0.04 s^{-1} and K_M = 21 ± 1.9 μM for S167A,[3] which is similar to that for rhIDO (k_{cat} = 1.4 ± 0.05 s^{-1}, K_M = 7 ± 0.8 μM). The corresponding values for S167H were k_{cat} = 0.006 ± 0.28 × 10^{-5} s^{-1} and K_M = 26 ± 1.3 μM, showing that S167H is effectively inactive for oxidation of L-Trp. A steady-state analysis at fixed concentration of substrate and varying concentration of O_2 was carried out to extract a K_M for O_2 binding to

[2] The xanthine/xanthine oxidase method produces a slightly different value than that obtained by potentiometric titration [−30 mV (*5*)]. We have observed slightly different values for reduction potentials of other heme proteins determined by the xanthine/xanthine oxidase method and other electrochemical methods (*9*). The discrepancy probably arises from the use of dithionite as a reductant in the potentiometric technique. Dithionite, a strong reducing agent, transfers all electron equivalents immediately to the protein, with subsequent equilibration assisted by mediators after equilibration at each potential; the next addition of dithionite corresponding to another potential requires a new equilibration. In the xanthine/xanthine oxidase method, xanthine oxidase feeds electrons slowly to the protein and the dye, so that equilibrium is reached at any point during the experiment. As an important control, experiments on rhIDO using different dyes gave the same value for the reduction potential [$E^{o\prime}(Fe^{3+}/Fe^{2+})$ = −63 mV using methylene blue; $E^{o\prime}(Fe^{3+}/Fe^{2+})$ = −68 mV using nile blue chloride].

[3] A k_{cat} of 1.95 ± 0.08 s^{-1} has been reported for S167A (*1*), but no K_M was reported.

Table 2: Kinetic and Thermodynamic Parameters for Binding of L-Trp and Cyanide to Ferric and of O_2 to Ferrous rhIDO, S167A, and S167H (50 mM Tris-HCl, pH 8.0, 25.0 °C)

variant	parameter	rhIDO	S167A	S167H
tryptophan	K_D (μM)	285 ± 6	8000 ± 1000[d]	6900 ± 1100[d]
	K_D (μM) (with CN)	16.4 ± 1.5[a]	992 ± 200[e]	ND[f]
	k_{on} (μM^{-1} s^{-1})	15500 ± 350	15000 ± 16700	5930 ± 150
	k_{off} (s^{-1})	9.1 ± 0.6	61 ± 2.7	41.6 ± 4
cyanide	K_D (μM)	3.57 ± 0.37[b]	1.92 ± 0.17	594 ± 30
	k_{on} (μM^{-1} s^{-1})	0.0214 ± 0.0006	0.1708 ± 0.0032	0.0004 ± 1.2 × 10^{-5}
oxygen	k_{on} (μM^{-1} s^{-1})	0.53 ± 0.006[c]	0.25 ± 0.002	0.11 ± 0.02
	k_{off} (s^{-1})	6.8 ± 1.8[c]	6.96 ± 8.2	3.03 ± 3.7
	k_{off}/k_{on} (=K_D)[g]	12.8 ± 3.53	27.8 ± 33	27.5 ± 38.5

[a] rhIDO was fully saturated with cyanide (80 μM) before addition of L-Trp. [b] There are no reported binding constants for cyanide binding to rhIDO, although Sono et al. have reported binding of cyanide to rabbit IDO [K_D = 11 μM (*19*)]. [c] Rate constants for binding of O_2 to rhIDO have not been reported previously. [d] Errors on these values are larger because the limited solubility of L-Trp in solution (maximum concentration ≈50 mM) means that larger volumes are needed during the titration and corrections for this dilution were necessary. [e] S167A was fully saturated with cyanide (20 μM cyanide)) before addition of L-Trp. [f] ND, K_D could not be measured because the spectral changes upon addition of L-Trp were too small to monitor. [g] These are calculated values and have higher errors because they use the k_{off} values which have large errors themselves (since they derive from an intercept on the k_{obs} versus concentration plot).

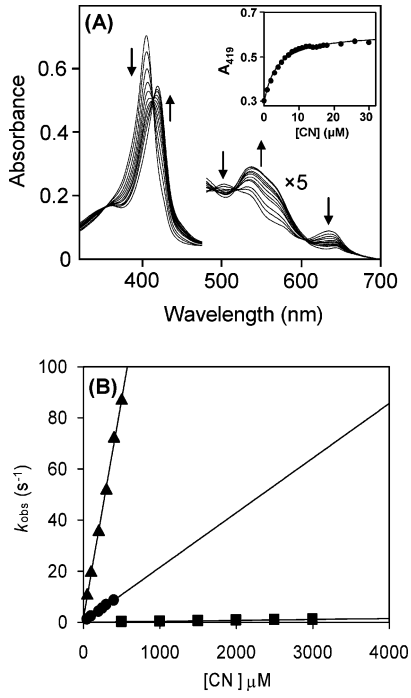

FIGURE 4: (A) Representative data set for the determination of K_D for binding of CN to rhIDO at pH 8.0. The arrows indicate the direction of change in absorbance upon successive additions of CN. Absorbance values in the visible region have been multiplied by a factor of 5. (Inset) Fit of binding data at 419 nm (according to eq 1 in ref *4*). (B) Concentration dependence of the observed rate constants of cyanide binding to ferric rhIDO (●), S167A (▲), and S167H (■). Linear regression analysis of the data yielded an apparent association constant (k_{on}) from the slope and a dissociation rate constant (k_{off}) from the ordinate intercept.

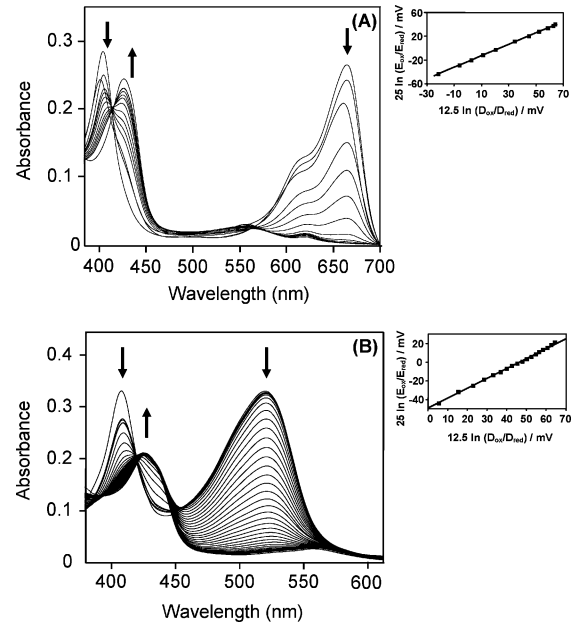

FIGURE 5: Family of spectra collected during determination of Fe^{3+}/Fe^{2+} reduction potential for (A) S167A with methylene blue and (B) S167H with phenosafranine. Conditions: 50 mM potassium phosphate, pH 7.0. Arrows indicate the direction of absorption changes at various parts of the spectrum during the reductive titration. (Inset) The corresponding linear Nernst plot.

rhIDO. This yielded a plot of reaction rate against O_2 concentration that was sigmoidal and did not follow typical Michaelis–Menten kinetics (data not shown). This may be a consequence of the complex nature of the assay mixture (an ascorbate/methylene blue reducing system, plus catalase). However, the rate of formation of *N*-formylkynurenine was independent of O_2 concentration above 150 μM, which suggests that at this concentration enzyme is saturated with O_2; we estimate therefore that the K_M for O_2 is <50 μM.

Formation and Decay of the Catalytic Ferrous−Oxy Intermediate. Spectroscopic changes observed on reaction of rhIDO, S167A, and S167H with O_2 were monitored using stopped-flow photodiode array spectroscopy. For rhIDO, the data were collected over a period of 1 s from the mixing event and were best fitted to a one-step model (A → B, Figure 6A and inset) in which species A (solid line) clearly represents the ferrous form of rhIDO (λ_{max} = 425, 527 sh, 558 nm) and species B (dotted line) has spectral properties characteristic of the ferrous−oxy rhIDO complex (λ_{max} = 416, 539, 576 nm). The ferrous−oxy complex was also observed for S167A and S167H, and both variants exhibited similar wavelength maxima to that seen for rhIDO (Table 1).

The concentration dependence of the rate constant (k_{obs}) for ferrous−oxy complex formation in rhIDO and the Ser 167 mutants was monitored at 416 nm using the single-wavelength mode of the stopped-flow apparatus. The corresponding rate constants for O_2 binding (k_{on}, k_{off}, eq 1) to rhIDO, S167A, and S167H are given in Table 2, and data are shown in Figure 6B. Similar values for k_{on} and k_{off} and the derived K_D were found for rhIDO and S167A (Table 2).

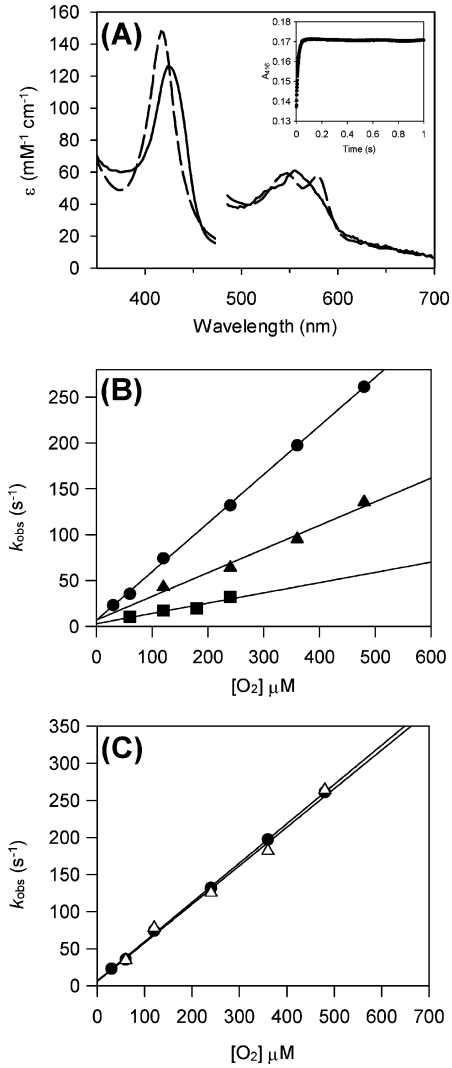

FIGURE 6: Reaction of rhIDO with O_2 monitored by stopped-flow spectroscopy. (A) Deconvoluted spectra for the time-dependent spectral changes on mixing 1 μM ferrous rhIDO with 130 μM O_2 (time base of 1 s). The data were fitted to a single-step model, A $\rightarrow$ B, with a rate constant (obtained from global fitting) of 75.4 $\pm$ 0.3 s^{-1}. (Inset) Absorption transient at 416 nm observed upon mixing of 1 μM ferrous rhIDO with 130 μM O_2. (B) Concentration dependence of the observed rate constant (k_{obs}) of O_2 binding to ferrous rhIDO (●), S167A (▲), and S167H (■). (C) Concentration dependence of the observed rate constant (k_{obs}) of O_2 binding to ferrous rhIDO in the absence (●) and presence of 300 μM 1-methyl-Trp (▲).

These ferrous−oxy complexes spontaneously decompose to ferric enzyme for all three proteins under anaerobic conditions (monitored at 576 nm). For S167H, the ferrous−oxy complex was particularly unstable, as evidenced by the half-life for this variant ($t_{1/2}$ = 0.7 s), which is much faster than the corresponding half-lives of both rhIDO and S167A ($t_{1/2}$ = 36 and 47 s, respectively).

It is not possible to determine a rate constant for reaction of O_2 with rhIDO in the presence of L-Trp under pre-steady-state conditions, because turnover occurs during the experiment. Instead, the rate constant was determined in the presence of excess 1-methyl-Trp (as a substrate analogue), which is a potent inhibitor of IDO (*13*). The data are shown in Figure 6C, which yields values for k_{on} and k_{off} of 0.52 $\pm$ 0.03 μM^{-1} s^{-1} and 6 $\pm$ 9 s^{-1}, respectively, and were very similar to the values calculated for O_2 binding to the ferrous enzyme alone (Table 2).

Detection of Intermediate Species during Reaction of Fe^{2+} with L-Trp and O_2. The above data clearly show that the S167H variant is unable to form a ferrous−oxy complex that is as stable as that observed for both rhIDO and S167A. We therefore sought to establish whether this instability was the source of the poor catalytic activity of S167H in the steady state. This was achieved by monitoring spectroscopic changes (by stopped flow) during the course of the catalytic reaction of S167H and comparing them to those observed for rhIDO.

rhIDO was incubated with O_2 for a period of 1 s (to allow for formation of the ferrous−oxy complex) and then mixed with excess L-Trp, and the spectral changes were monitored for 50 s. The first spectrum (collected at 1.28 ms after mixing of L-Trp) clearly represents the enzyme in the ferrous−oxy form [Figure 7A (solid line), λ_{max} = 416, 539, 576 nm]. For the next 0.75 s no major spectral change was observed [apart from a small (2 nm) shift in the Soret peak from 416 to 414 nm], and no *N*-formylkynurenine was detected as evidenced by a lack of absorbance change at 321 nm (Figure 7A, inset). We therefore propose that this species represents the ternary [enzyme−O_2−Trp] complex [Figure 7A (dashed line), λ_{max} = 414, 544, 576 nm]. A ternary complex with similar characteristics (λ_{max} = 413, 541, 576 nm) has been observed previously under nonphysiological conditions(low temperature and cryogenic solvent) (*14*). During the steady-state phase, formation of *N*-formylkynurenine is apparent as there is a linear increase in absorbance at 321 nm over 5 s (Figure 7A, inset). The spectrum of the species present during the steady-state phase is similar to that of the proposed ternary complex [Figure 7A (dotted line), λ_{max} = 413, 543, 576 nm].

When the experiment was repeated but ferrous rhIDO was incubated with L-Trp first and then mixed with O_2, the first spectrum after final mixing was in this case identified as a ferrous−Trp complex [Figure 7B (solid line), λ_{max} = 413, 551, 575 (sh) nm]. After 0.75 s, the next species identified [Figure 7B (dashed line)] had a spectral form identical to that seen above, and we therefore assign it as arising from the ternary [enzyme−O_2−Trp] complex. The steady-state intermediate [Figure 7B (dotted line)] that was detected was also identical to that observed in the experiment above. These two experiments indicate that, regardless of the order of mixing, a species is identified in rhIDO that closely resembles a ferrous−oxy intermediate and that we assign as the catalytic ternary complex.

Parallel experiments with S167H were also carried out. In the first experiment, ferrous S167H was mixed first with O_2, and after a predetermined period of time (typically 0.8 s) the solution was mixed with excess L-Trp and the spectral changes were monitored over a period of 500 s. The first species observed, 2.56 ms after mixing with L-Trp [Figure 7C (solid line), λ_{max} = 416, 543, 581 nm], is clearly identified as the ferrous−oxy form of the enzyme. Within 0.5 s, this ferrous−oxy species has decayed, and a second species with a blue-shifted Soret band and a broad band in the visible region [λ_{max} = 412, 433 (sh), 553 nm] was detected [Figure 7C (dashed line)]; no product formation had occurred at this point (as shown by the absence of an absorbance change at 321 nm; Figure 7C, inset). This species is different from the corresponding species in rhIDO that was assigned as arising from the ternary complex [Figure 7A (dashed line)]. The

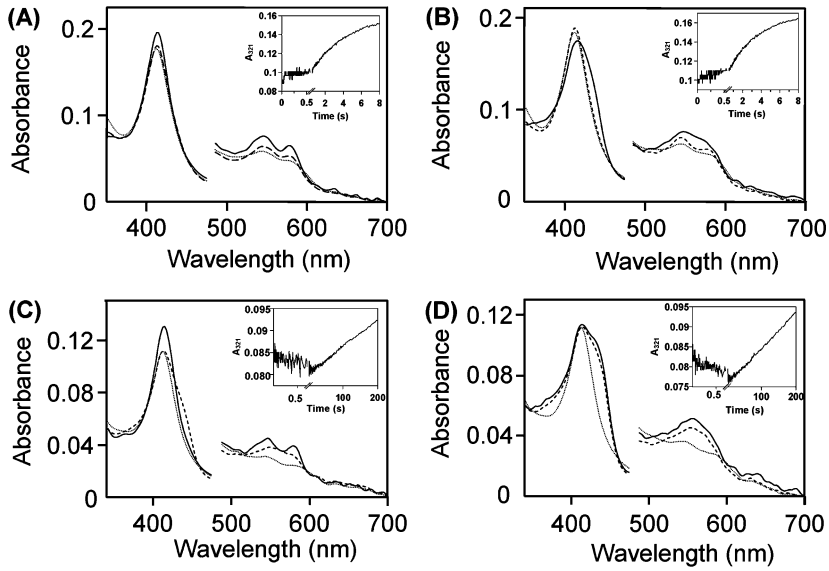

FIGURE 7: Detection of steady-state intermediates. (A) rhIDO premixed with O_2 followed by mixing with L-Trp. (B) rhIDO premixed with L-Trp followed by mixing with O_2. (C) S167H premixed with O_2 followed by mixing with L-Trp. (D) S167H premixed with L-Trp followed by mixing with O_2. (Inset) Time dependence of absorbance changes at 321 nm, which report on *N*-formylkynurenine formation. Absorbance values in the visible region have been multiplied by a factor of 3. For (A) and (B), the solid line shows the spectrum at 1.28 ms, the dashed line at 0.75 s, and the dotted line at 5 s; for (C) and (D), the solid line shows the spectrum at 2.56 ms, the dashed line at 0.5 s, and the dotted line at 100 s.

Scheme 2: Schematic Diagram of the Possible Hydrogen-Bonding Interactions (Dashed Lines) to a Bound Diatomic Ligand (either O_2 or CN, Represented by AB) in IDO (*2*)[a]

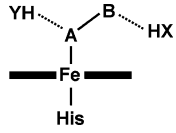

[a] Hydrogen bond donors are indicated as XH and YH and are envisaged as being provided by either active site water molecules or substrate. Although water molecules are not present in the crystal structure of rhIDO (*1*), the actual hydration structure is likely to be different since the crystal structure contained two CHES molecules and the inhibitor 4-phenylimidazole in the active site, neither of which would be present physiologically.

final spectrum [Figure 7C (dotted line)] is typical of the species observed during the steady-state phase of the reaction (λ_{max} = 412, 543, 577 nm), but the intensities are reduced when compared to the corresponding steady-state intermediate in rhIDO [Figure 7A (dotted line)]. During this steady-state phase, *N*-formylkynurenine formation is observed as a linear increase in absorbance at 321 nm (Figure 7C, inset). Note the differences in time scales for product formation in rhIDO (5 s) and S167H (200 s) (insets to panels A and C of Figure 7, respectively).

In the second experiment, ferrous S167H was incubated first with L-Trp, and then this complex was mixed with O_2. The first species observed 2.56 ms after mixing with O_2 [λ_{max} = 414, 549 nm, Figure 7D (solid line)], by comparison with rhIDO above (Figure 7B solid line), we assign as arising from the ferrous−Trp complex. After 0.5 s (when *N*-formylkynurenine has not yet been formed) a second species was identified [λ_{max} = 412, 425 (sh), 553 nm, Figure 7D (dashed line)] which is similar to that observed at the same time point in Figure 7C. During the steady-state phase, *N*-formylkynurenine formation is observed as a linear increase in absorbance at 321 nm (Figure 7D, inset), and the intermediate that is detected at this point [Figure 7D (dotted line)] is identical to that in Figure 7C (dotted line). At no stage is clear formation of a ferrous−oxy species observed.

These experiments for S167H indicate (i) that the proposed ternary complex identified for rhIDO above is not observed in S167H and (ii) that the species present in the steady state for S167H is not the same as that for rhIDO nor does it resemble a ferrous−oxy species (as for rhIDO), regardless of the order of mixing.

DISCUSSION

Our intention in this paper was to make comparisons between the active site structures of different mammalian and bacterial heme dioxygenases and to use this as a basis for developing our ideas on the reaction mechanism in these enzymes. Below we discuss the implications of these data in terms of our broader understanding of substrate binding and catalysis across the heme dioxygenase family; we include direct comparisons with human TDO (*4*).

Hydrogen-Bonding Interactions in the Active Site of IDO. Electronic spectra for the ferrous form of S167A are similar to the those of wild-type protein and indicate that this variant is 5-coordinate (as for rhIDO). In accordance with this, the ferrous−oxy derivative forms normally (as evidenced by k_{on}, k_{off}) and decays with a half-life ($t_{1/2}$ = 47 s) that is essentially the same as that for rhIDO ($t_{1/2}$ = 37 s). Since the steady-state data indicate that S167A binds (as evidenced by K_M) and turns over (k_{cat}) substrate essentially as normal, the immediate conclusion is that Ser167, which is the only polar residue in the IDO active site (Figure 1), is not important either for binding of O_2, for stabilization of the ferrous−oxy complex, or for conversion of the substrate to *N*-formylkynurenine.

There are no other potential hydrogen-bonding residues in the active site of IDO (Figure 1). This is in contrast to the globins, in which a distal histidine residue is located

Scheme 3: Possible Reaction Mechanisms for the Conversion of L-Trp to *N*-Formylkynurenine Catalyzed by IDO and TDO

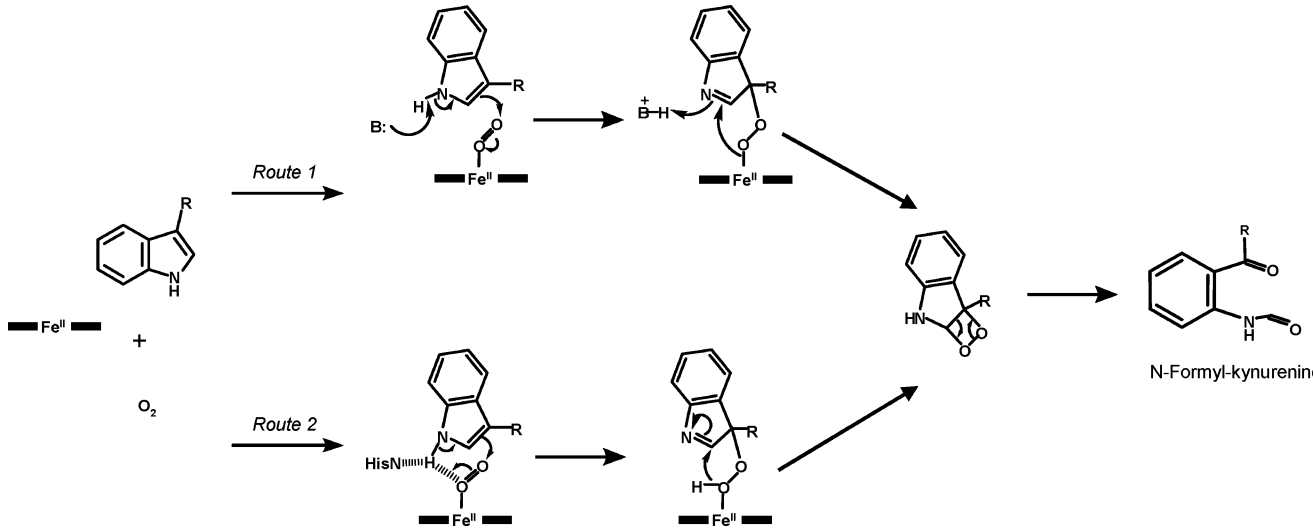

directly above the iron and is poised to hydrogen bond to the bound O_2. We therefore interpret these data to mean that any hydrogen-bonding stabilization of the bound O_2 ligand in IDO is most likely through an active site water molecule(s), as occurs in some other catalytic O_2 binding proteins (e.g., heme oxygenase and cytochrome P450). In this context, we note that $k_{on(O_2)}$(rhIDO) $\approx 2k_{on(O_2)}$(S167A): if binding of O_2 involves electron transfer and formation of a ferric−superoxide species, then $k_{on(O_2)}$(rhIDO)/$k_{on(O_2)}$(S167A) = exp[($E^\circ_{rhIDO} - E^\circ_{S167A}$)/2$RT$] = 2.7, which is close to the observed value of 2. The similarity in values suggests that differences in k_{on} can be accounted for by the differences in potential, assuming that the binding event involves electron transfer. In other words, the kinetic and thermodynamic data support the idea of a hydrogen-bonding network involving water molecules since movement of electron density onto O_2 would be expected to involve hydrogen bonding from O_2 to a hydrogen bond donor.

The precise mode of substrate binding in IDO is not yet known, but we envisage that in the presence of L-Trp these hydrogen-bonding interactions to O_2 are replaced with hydrogen bonds to the substrate (Scheme 2). This would also account for the fact that the affinity of L-Trp for both ferric rhIDO and ferric S167A is considerably enhanced in the presence of cyanide (Table 2), where these hydrogen-bonding interactions to the substrate are also presumably possible (Scheme 2).

Comparisons with Bacterial and Human TDOs: S167H Variant. In xTDO, Ser167 is replaced with a histidine residue (His55, Figure 1). Sequence alignments with human TDO indicate that it also has a His at this position (His76). In the following sections, we compare the properties of the S167H variant with these other two dioxygenases.

The spectroscopic and ligand binding data indicate that the ferric derivative of the S167H variant most likely has His167 bound to the iron but that this is displaceable on binding of other strong ligands (e.g., cyanide) or on reduction. Hence, although the new ligand is not located directly "above" the heme (as in other bishistidine ligated heme proteins such as cytochrome b_5), it appears that His167 is within bonding distance of the heme. This is in contrast to the presumed coordination geometry in human TDO, which contains a histidine (His76) at the position equivalent to Ser167, for which spectroscopic data indicate mainly a high-spin, water-bound heme species in the ferric form (*4*). We conclude that there are differences in the precise orientation of the histidine residue between the two enzymes, such that coordination to the heme occurs in one case but not the other.

Comparisons with Bacterial and Human TDOs: Stability of the Ferrous−Oxy Complex. The ferrous−oxy complex of S167H is very greatly destabilized compared to rhIDO. This behavior for S167H replicates that in *Pseudomonas* TDO (*15*) and in recombinant human TDO (*4*), where the ferrous−oxy complex is similarly unstable. The very low reduction potential for S167H (−203 mV) is certainly likely to be influential in destabilizing the ferrous−oxy complex but does not provide a complete explanation because the reduction potential of recombinant human TDO (−92 mV) is higher and in this enzyme the ferrous−oxy species is not detected at all (*4*). By way of comparison, reduction potentials for myoglobin, in which the ferrous−oxy complex is much more stable, are typically in the range of ≈+50 mV (*16*). The absence of potential hydrogen-bonding residues within the active site of IDO and the presumed failure of IDO to duplicate the stabilizing hydrogen-bonding interactions observed in the globins (*vide supra*) might also be influential, however.

The poor stability of the ferrous−oxy complex in S167H is reflected in the fact that the enzyme has lost >99% of its activity (as evidenced by k_{cat}), although we note that it binds L-Trp normally (as evidenced by K_M). The formation of the ferrous−oxy complex is an important junction in the overall dioxygenase mechanism: this intermediate needs to be stable enough to interact with the substrate so that effective conversion to product can occur. Our stopped-flow kinetic data for rhIDO in the steady state indicate that significant amounts of the ferrous−oxy complex are present under turnover conditions. For S167H this is not the case, however; this presumably reflects the rapid and unproductive decay of the ferrous−oxy species, which then competes with the slower (productive) conversion of substrate to product.

Mechanistic Implications. Our kinetic data for rhIDO reveal that the enzyme shows no substantial preference for binding of O_2 over L-Trp because the steady-state K_M for O_2 (which is consistent with the K_D determined under pre-

steady-state conditions) is in a similar range to the K_M for L-Trp binding. Also, the kinetic data with 1-methyl-Trp show no enhancement of affinity for O_2 in the presence of this substrate analogue. By implication we conclude that substrate binding does not preferentially favor O_2 binding in rhIDO. This is consistent with our pre-steady-state data in which we observe a catalytic intermediate, proposed as the ternary enzyme−O_2−Trp complex, at the same point in the reaction mechanism regardless of whether O_2 or L-Trp is mixed with the enzyme first.

There are two possible mechanisms for initial reaction of the ferrous−oxy complex with bound substrate (Scheme 3). One mechanism involves base-catalyzed abstraction of the indole NH (route 1); the other does not (route 2). Early suggestions (*13*) favored the base-catalyzed mechanism. However, there is no evidence from our data that the only polar residue present in the active site of rhIDO, Ser167, plays any role in controlling the reaction mechanism. The alternative route (route 2) does not involve base-catalyzed proton abstraction (*17*). However, in xTDO the N^{ϵ} of His55 is hydrogen bonded to the indole nitrogen of the bound substrate (Scheme 3), and although removal of this residue (H55A) lowers activity ($k_{cat(H55A)} = 0.1k_{cat(wild\ type)}$ (*2*)), some activity remains, indicating that catalysis still occurs even in the absence of His55. This would be consistent with the fact that His55 is not needed in IDO and is replaced with Ser167. Further, it would mean that the most likely role for His55 is not in base-catalyzed abstraction but in orienting the indole proton, through hydrogen bonding, in a suitable position for deprotonation (although we note that the pK_a for the indole nitrogen of L-Trp in solution ($pK_a = 16.9$ (*18*)) is out of range and would need to decrease substantially in the enzyme–substrate complex). Presumably, the same interaction exists in human TDO (through His76).

ACKNOWLEDGMENT

We thank Dr. P. Jenkins, Dr. B. Rawlings, and Dr. I. K. Macdonald for helpful discussions.

REFERENCES

1. Sugimoto, H., Oda, S., Otsuki, T., Hino, T., Yoshida, T., and Shiro, Y. (2006) Crystal structure of human indoleamine 2,3-dioxygenase: catalytic mechanism of O_2 incorporation by a heme-containing dioxygenase. *Proc. Natl. Acad. Sci. U.S.A. 103*, 2611–2616.
2. Forouhar, F., Anderson, J. L., Mowat, C. G., Vorobiev, S. M., Hussain, A., Abashidze, M., Bruckmann, C., Thackray, S. J., Seetharaman, J., Tucker, T., Xiao, R., Ma, L. C., Zhao, L., Acton, T. B., Montelione, G. T., Chapman, S. K., and Tong, L. (2007) Molecular insights into substrate recognition and catalysis by tryptophan 2,3-dioxygenase. *Proc. Natl. Acad. Sci. U.S.A. 104*, 473–478.
3. Dick, R., Murray, B. P., Reid, M. J., and Correia, M. A. (2001) Structure-function relationships of rat hepatic tryptophan 2,3-dioxygenase: identification of the putative heme-ligating histidine residues. *Arch. Biochem. Biophys. 392*, 71–78.
4. Basran, J., Rafice, S., Chauhan, N., Efimov, I., Cheesman, M. R., Ghamsari, L., and Raven, E. L. (2008) A kinetic, spectroscopic, and redox study of human tryptophan 2,3-dioxygenase. *Biochemistry 47*, 4752–4760.
5. Papadopoulou, N. D., Mewies, M., McLean, K. J., Seward, H. E., Svistunenko, D. A., Munro, A. W., and Raven, E. L. (2005) Redox and spectroscopic properties of human indoleamine 2,3-dioxygenase and a His303Ala variant: implications for catalysis. *Biochemistry 44*, 14318–14328.
6. Antonini, M., and Brunori, E. (1971) *Hemoglobin and Myoglobin and their Reactions with Ligands*, North Holland Publishers, Amsterdam.
7. Patel, N., Jones, D. K., and Raven, E. L. (2000) Investigation of the haem-nicotinate interaction in leghaemoglobin. Role of hydrogen bonding. *Eur. J. Biochem. 267*, 2581–2587.
8. Massey, V. (1991) *Flavins and Flavoproteins* (Curti, B., Ronchi, S., and Zanetti, G., Eds.) pp 59–66, Walter de Gruyter, New York.
9. Efimov, I., Papadopoulou, N. D., McLean, K. J., Badyal, S. K., Macdonald, I. K., Munro, A. W., Moody, P. C., and Raven, E. L. (2007) The Redox Properties of Ascorbate Peroxidase. *Biochemistry 46*, 8017–8023.
10. Binstead, R. A., and Zuberbuehler, A. D.,Specfit, Chapel Hill, NC.
11. Gadsby, P. M., and Thomson, A. J. (1990) Assignment of the axial ligands of ferric ion in low-spin hemoproteins by near-infrared magnetic circular dichroism and electron paramagnetic resonance spectroscopy. *J. Am. Chem. Soc. 112*, 5003–5011.
12. More, C., Belle, V., Asso, M., Fournel, A., Roger, G., Guigliarelli, B., and Bertrand, P. (1999) *Biospectroscopy S5*, S3–S18.
13. Sono, M., Roach, M. P., Coulter, E. D., and Dawson, J. H. (1996) Heme-containing oxygenases. *Chem. Rev. 96*, 2841–2888.
14. Sono, M. (1986) Spectroscopic and equilibrium properties of the indoleamine 2,3-dioxygenase-tryptophan-oxygen ternary complex and of analogous enzyme derivatives. Tryptophan binding to ferrous enzyme adducts with dioxygen, nitric oxide, and carbon monoxide. *Biochemistry 25*, 6089–6097.
15. Ishimura, Y., Nozaki, M., and Hayaishi, O. (1970) The oxygenated form of L-tryptophan 2,3-dioxygenase as reaction intermediate. *J. Biol. Chem. 245*, 3593–3602.
16. Raven, E. L., and Mauk, A. G. (2001) Chemical reactivity of the active site of myoglobin. *Adv. Inorg. Chem. 51*, 1–49.
17. Terentis, A. C., Thomas, S. R., Takikawa, O., Littlejohn, T. K., Truscott, R. J., Armstrong, R. S., Yeh, S. R., and Stocker, R. (2002) The heme environment of recombinant human indoleamine 2,3-dioxygenase. Structural properties and substrate-ligand interactions. *J. Biol. Chem. 277*, 15788–15794.
18. Yagil, G. (1967) The proton dissociation constant of pyrrole, indole, and related compounds. *Tetrahedron 23*, 2855–2861.
19. Sono, M. (1989) Enzyme kinetic and spectroscopic studies of inhibitor and effector interactions with indoleamine 2,3-dioxygenase. 2. Evidence for the existence of another binding site in the enzyme for indole derivative effectors. *Biochemistry 28*, 5400–5407.

BI702405A